EFFECTS OF COATING STRUCTURE BY Al_2O_3 NANOPARTICLES DEPOSITION ON CRITICAL HEAT FLUX OF R123 IN FLOW BOILING

Seok Bin Seo and In Cheol Bang*
School of Mechanical and Nuclear Engineering
Ulsan National Institute of Science and Technology (UNIST)
50 UNIST-gil, Ulju-gun, Ulsan, 689-798, Republic of Korea
icbang@unist.ac.kr

ABSTRACT

In this study, R-123 flow boiling experiments were carried out to investigate the effects of nanoparticle deposition on heater surfaces on flow CHF and boiling heat transfer. It is known that CHF enhancement by nanoparticles results from porous structures. Although previous studies have investigated the surface effects through surface modifications, most studies are limited to pool boiling conditions and so the porous effects in flow boiling heat transfer are still unclear. This paper focused on the porous effects on CHF in flow boiling. In this study R123 was used to investigate the CHF and boiling mechanisms. Bare and Al_2O_3 nanoparticles-coated surfaces were prepared for the experiments. The CHF of each surface was measured with different mass fluxes of 1600, 1800, 2100, 2400 and 2600 kg/m^{2}s. The nanoparticles-coated tube showed CHF enhancement up to 17% at 2400 kg/m^{2}s mass fluxes compared to the bare tube. The factors for CHF enhancement are related to the enhanced rewetting process derived from capillary action through porous structures built-up by nanoparticles suppressing wettability since highly wettable R123 refrigerant was used as a working fluid.

KEYWORDS
Boiling heat transfer, Critical Heat Flux, Crud, Porous structure, Nanofluid

1. INTRODUCTION

Boiling mechanism is an effective heat transfer mode for its high heat capacity through phase change. Many thermal applications, especially nuclear power plants, adopt boiling mechanism as a heat removal system. However, the heat removal performance using boiling mechanism is limited by a sudden and drastic reduction in the heat transfer coefficient, called critical heat flux (CHF). Because CHF can lead to a serious damage or even burnout of the heating surface, it is crucial that the nuclear reactors predict CHF and operate below CHF to prevent severe accidents resulted from failures of the reactor vessel. Thus, understanding CHF mechanism and increase in CHF provide additional safety margin for the reactor, and also enable power uprates in commercial nuclear power plants [1]. For the PWR, expecting CHF mechanism is called departure from nucleate boiling (DNB) whose characteristics are high mass flow rate and low quality. Thus it is necessary to understand the physical model of DNB for the safety margin of PWR.

Corresponding author: Tel:+82-52-217-2915, Fax:+82-52-217-3008
E-mail : icbang@unist.ac.kr (In Cheol Bang)

The widely accepted DNB models were proposed by Weisman and Pei [2] and Lee and Mudawwar [3]. One is the near-wall bubble crowding model based on enthalpy transportation through the interface between the boundary layer and the bulk core. The other is the liquid sublayer dryout model which introduces a liquid sublayer located between the vapor blanket and the heated surface. In the liquid sublayer dryout model, the dry patch is generated from the vapor blanket contacting the heated wall as a result of Helmholtz instability. Near CHF, the dry patch spreads over the wall, when the rate of sublayer mass loss by evaporation exceeds that of the liquid entering the sublayer from the core region.

Many techniques have been introduced to increase CHF in the nuclear reactor. Nanofluids are a recently-introduced technique enhancing the boiling heat transfer and CHF [4]. Early studies using different nanofluids have reported the significant enhancement of CHF in pool boiling up to 200% [5-9]. CHF enhancement by nanofluids in flow boiling also has been investigated, which is the situation of interest for nuclear applications [10-13]. Relatively few studies about flow boiling using nanofluids have reported up to 108% of CHF enhancement which is lower compared to that in pool boiling. Finally, they referred nanoparticles-deposited layer of the heating surface as main factors of CHF enhancement. However, the mechanism of CHF enhancement has yet to be clarified and is still under discussion.

Although nanofluid has been introduced as an effective technique to enhance CHF in flow boiling, its feasibility for nuclear applications seems to be low due to its stability and cleaning issues. Instead of nanofluid, nanoparticle-coated heating surface has been considered as an alternative method to obtain similar CHF enhancement without those issues. In addition, nanoparticle-coated heating surface can be more meaningful technique considering the existence of CRUD on the cladding surface in actual nuclear reactor. CRUD is corrosion products deposited on the cladding surface forming micro-layer structure during the normal operation of nuclear power plant [14]. Especially, CRUD in the range of 10-20μm thickness provides beneficial effects on the boiling heat transfer coefficient and CHF. In general, CRUD is a porous structure made of hydrophilic particles which is similar with nanoparticle-coated structures [15]. Thus, investigation of nanoparticle-coated structures can be further extended to CRUD structure leading to clear prediction of CHF enhancement in actual nuclear reactor.

Few studies focused on CHF enhancement by nanoparticle-coated surface in flow boiling condition. Sarwar et al. [16] conducted the flow boiling experiment measuring CHF on coated surface. The authors coated Al_2O_3 and TiO_2 nanoparticles inside the circular tube using coating paint technique. The resulted nanoparticles-coated surface showed porous structure which is similar with heating surfaces from previous nanofluid-boiled experiments. In addition, measured CHFs were enhanced up to 25% compared to those on the smooth tube. Truong et al. [17] also pre-coated Al_2O_3 nanoparticles inside the tube to investigate CHF enhancement. The test parameters included the coating concentration of the nanofluid, coating heat flux, and coating time. The maximum CHF enhancement occurred in the condition of the highest coating concentration, coating heat flux, and coating time with the value of 35%. Kim et al. [18] measured flow boiling CHFs in two conditions; Al_2O_3 nanofluid boiled through plain tube and pure water boiled through Al_2O_3 nanoparticle-coated tube. In both cases, CHFs were enhanced compared to CHF on water-boiled plain tube, and there was no big difference in CHF results between two conditions. These results confirmed that deposition of nanoparticles on the heating surface leads to the CHF enhancement.

While early studies have focused mainly on wettability of heating surface to investigate CHF enhancement mechanism, both surface morphology and wettability have been considered recently [9,11]. Because surface characteristics are closely coupled each other, it is crucial that those parameters are separated as much as possible. In that sense, present study used refrigerant R123 as a working fluid for CHF measurement. Although refrigerant R123 from previous studies has been used mainly for flow boiling in microtubes to investigate parametric effects and flow regime [19-21], this study used cylindrical tube in millimeter size to investigate CHF enhancement mechanism. Highly wettable characteristic of refrigerant was expected to suppress wettability effect of nanoparticle-coated heating

surface on CHF, then, surface morphology including porosity and roughness was assumed to be attributed to CHF enhancement [22]. Finally, in this study, CHF enhancement on Al_2O_3 nanoparticle-coated surface was measured with different mass flux conditions, and its mechanism would be analyzed based on previous CHF models in terms of liquid sublayer as follows.

2. EXPERIMENTAL PROCEDURE

The schematic diagram of experimental facility is shown in Fig. 1. The flow loop consists of a test section, a pump, a flow meter, a preheater, a condenser, and a fluid reservoir. Controlled volume pump is used for small mass flow rate range from 0.037 to 0.061 kg/s. Corresponding mass flux is the range from 1600 to 2800 kg/m^{2}s. The gear flow meter measures mass flow rate using rotating gears in liquid flow. After passing the mass flow meter, the coolant flows to the preheater to maintain constant inlet temperature. Condenser has capacity of 11kW enough to remove applied heat from test section. 1/4 inch Stainless Steel 316L tubes of 5.45 mm inner diameter were used as test heaters. The heating length is 280 mm. The working fluid is R123 which has lower boiling temperature of 26°C at atmosphere. The detailed test matrix of experiment is listed in table 1. The temperatures of fluid at the inlet and outlet of test section were measured by thermocouples of K-type, which were obtained by a data acquisition system. Another five K-type thermocouples are installed to measure the outside wall temperatures of tube. CHF occurs near the exit of the test section due to axially-uniform heat flux. When it takes place a wall temperature excursion, the heat flux value at that point becomes the CHF. The determination of CHF based on the wall temperature excursion is shown in Fig. 2.

Table 1. Test matrix of the experiment

Test section characteristics	
Geometry	SS316L cylindrical tube
Outer diameter	6.35mm
Inner diameter	5.45mm
Heated length	280mm
Surface conditions	
Bare	-
Coated	900s quenching with 0.01V% Al_2O_3 nanofluid
Vertically upward flow	
Pressure	1 bar
Mass flux	1600, 1800, 2100, 2400, 2600 kg/m^{2}s
Inlet subcooling	5°C
Working fluid	**R123**
Density	1460 kg/m^3 (liquid)
	6.41 kg/m^3 (vapor)
Latent heat	170.2 kJ/kg
Heat capacity	1.026 kJ/kgK

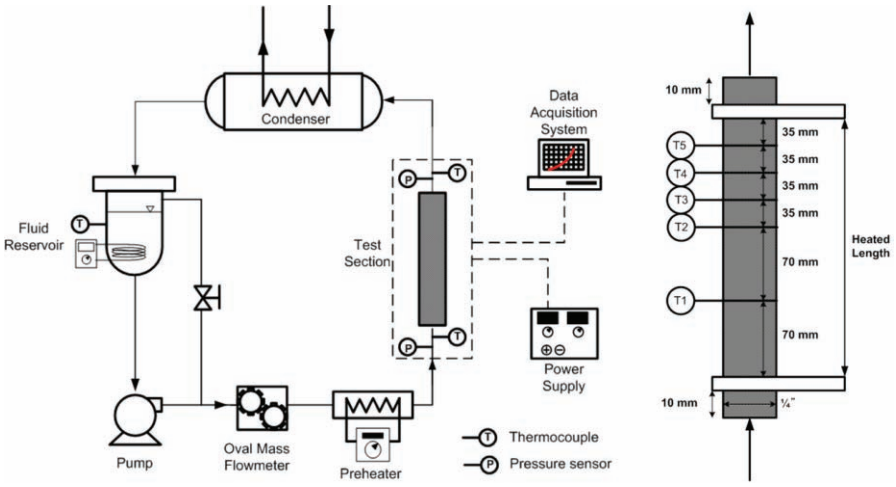

Figure 1. Schematic diagram of the testing apparatus.

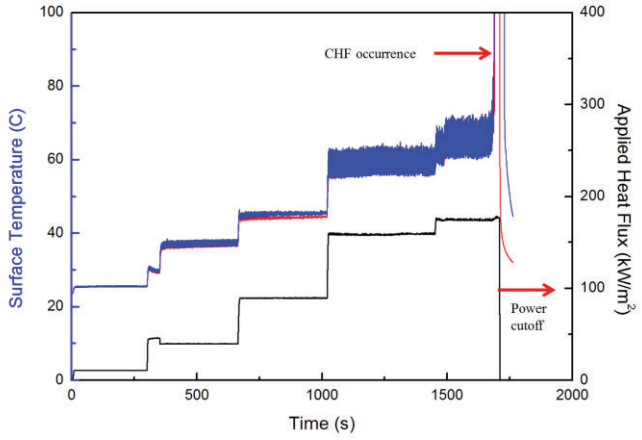

Figure 2. Wall temperature and heat flux history in a typical CHF run.

3. DATA REDUCTION AND UNCERTAINTIES

The voltage, current, inlet and outlet fluid temperatures, wall temperature, inlet and outlet pressures were measured. The electrical input power applied to the test section was determined with measured voltage and current from the power supply

$$P = V \times I \tag{1}$$

The inner wall temperature of the test section is calculated as

$$T_{wall} = T_{wall,out} - \dot{q}_t \frac{\ln(D_o / D_i)}{2\pi L_{eff,h} k_c} \tag{2}$$

where actual critical heat flux corresponded to inner surface area of test section is expressed as

$$q''_{eff} = \frac{P}{\pi D_i L} \tag{3}$$

Finally, the exit quality can be calculated with the mass flow rate and net power derived from the phase change as heat balance

$$X_e = \frac{1}{h_{fg}}\left(\frac{\dot{Q}_{net}}{\dot{m}_f} - c_{p,f}\left(T_{sat} - T_{in}\right)\right) \tag{4}$$

The uncertainties of temperature and flow rate are less than ±0.5°C and ±5%, respectively. In addition, the uncertainties in the electrical voltage, current, inner diameter, and length of test section are estimated to be ±0.3%, ±0.08%, ±0.1%, and ±1%, respectively. Finally, the uncertainty in the critical heat flux is evaluated as:

$$\frac{U_{q''}}{q''} = \sqrt{\left(\frac{U_V}{V}\right)^2 + \left(\frac{U_I}{I}\right)^2 + \left(\frac{U_{D_i}}{D_i}\right)^2 + \left(\frac{U_L}{L}\right)^2} \tag{5}$$

Therefore, the measurement uncertainty of the calculated critical heat flux is <±1.05%.

4. CHARACTERIZATION OF NANOPARTICLES-COATED SURFACE

In general, the major parameters to characterize a surface treatment are wettability, roughness and porosity as well as permeability and capillarity. The capillary action or capillarity relationship depends on the interaction of wettability, pore structure, initial saturation and saturation history which are liquid distribution inside the pore structure [23]. No simple relationship exists that relates the capillary pressure determined at two different wettabilities. The surface effects on boiling heat transfer and CHF mechanisms are summarized in Table 2.

Table 2. Summary of the major surface parameters on boiling heat transfer and CHF mechanism

Surface Parameters	Characteristics	Quantification (measurement)
Wettability	Determines the wetting zone on the surface, rewetting	Contact angle (°)
Roughness	Affects the number of active nucleation sites on the surface Increases active boiling center Amplifies for wettability	Surface's vertical Deviation (m)
Porosity	Increases the nucleation site density Enhances transport of liquid between nucleation sites Thick porous layer can role as additional thermal resistance	void fraction
Permeability	The property of pore structure that is an indication of the ability for gases or fluids to flow through the structure	Forced liquid flow (m^2)
Capillarity	Affects liquid supply to the dry patches on the surface induced by the capillary action	Capillary height or length (m)

In this study, nanoparticles were coated on the inner surface of tube through a quenching facility at UNIST. Previous studies with quenching method at UNIST have shown the stability and maintenance of nanoparticle-coated structure inside the tube [24]. To coat Al_2O_3 nanoparticles inside the tube, 0.01 vol% nanofluids were injected at 3 cm/s flow rate into preheated test section (600 – 650 °C) to deposit the nanoparticles on the inner surface of the test section. The circulation of nanofluids last for 900 s. The uncertainties of thermocouple and flow rate are less than 0.1°C, 5% respectively. The boiling process induces the nanoparticles-coating on the test section. And the adhesion force is significant to maintain the deposition of nanoparticles on the surface against the flow of water.
Fig. 3 shows SEM images of the bare and nanoparticle-coated test sections. Compared to the bare surface like Fig. 3 (a), Al_2O_3 nanoparticles-coated surfaces show a number of pores on the surface as shown in Fig. 3 (b). Also, from Figs. 3(b) and 3(c), it is certain that the deposited nanoparticles almost remained for all the experiments. From perspective view of nanoparticle-coated surface shown in Fig. 4, nanoparticles-coated structure shows very rough surface, which can be assumed to give higher roughness value compared to bare surface.

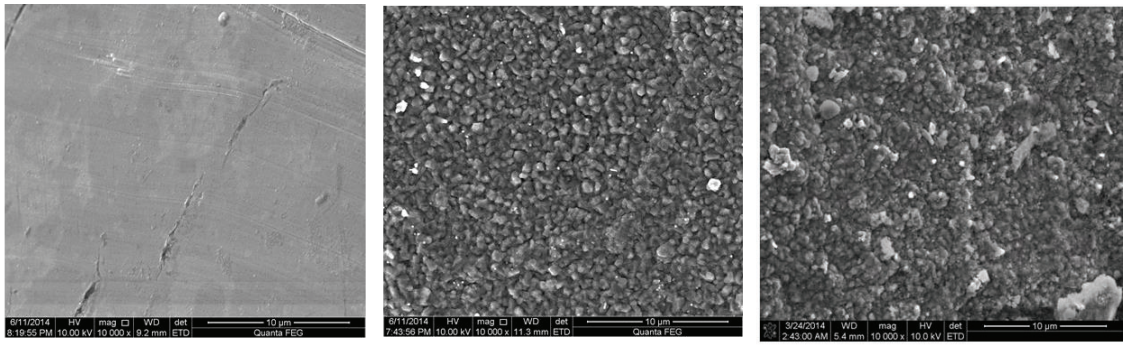

(a) (b) (c)

Figure 3. SEM images of test section: (a) Bare surface; (b) Al_2O_3 nanoparticle-coated surface before the experiment; (c) Al_2O_3 nanoparticle-coated surface after the experiment.

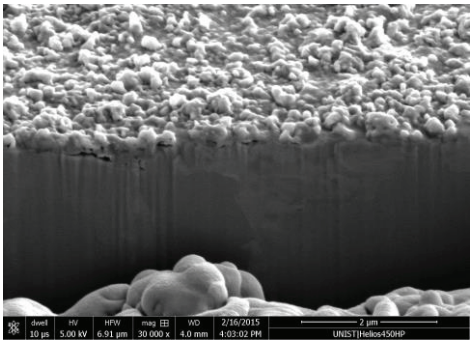

Figure 4. Cross sectional view of Al_2O_3 nanoparticle-coated surface using FIB technique.

The R123 droplets on the bare and nanoparticles-coated surfaces as specimens were used to measure the static contact angle. The static contact angle for bare surface was 20.5° while those for nanoparticles-coated surfaces were 22.3° and, respectively. It indicates that R123 shows very high wetting performance on both bare and nanoparticles-coated tubes. The measured static contact angles are shown in Fig. 5.

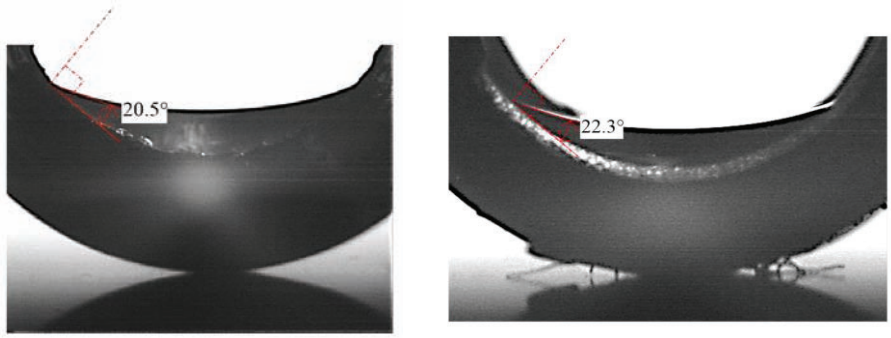

(a) **(b)**

Figure 5. Static contact angle of R123: (a) bare surface; (b) Al_2O_3 nanoparticle-coated surface.

5. RESULTS AND DISCUSSION

In this paper, the effects of nanoparticles depositions on flow boiling CHF using R123 were investigated. The mass flux conditions (G) are of 1600, 1800, 2100, 2400, 2600 kg/m^{2}s at inlet subcooled temperature of 5°C. Based on liquid sublayer model, CHF enhancement by nanoparticles-coated surface is analyzed.

Flow boiling experiments in R123 were conducted on bare and nanoparticles-coated heaters at given mass fluxes. Each heat flux versus wall temperature data was plotted at each mass flux. The obtained boiling curves at different mass flux are shown in Fig. 6. As the mass flux increases, the heat transfer coefficient which refers the slope of boiling curve also increases. For all mass flux conditions, the heat transfer coefficients of bare tube and Al_2O_3 nanoparticle-coated tube show little differences. Considering that heat transfer coefficient is highly dependent on surface wettability and coating layer thickness, and little on surface morphology [25], nano-scaled coating layer with highly wettable R123 in this study gives little effects on the heat transfer coefficients of bare and Al_2O_3 nanoparticle-coated tube.

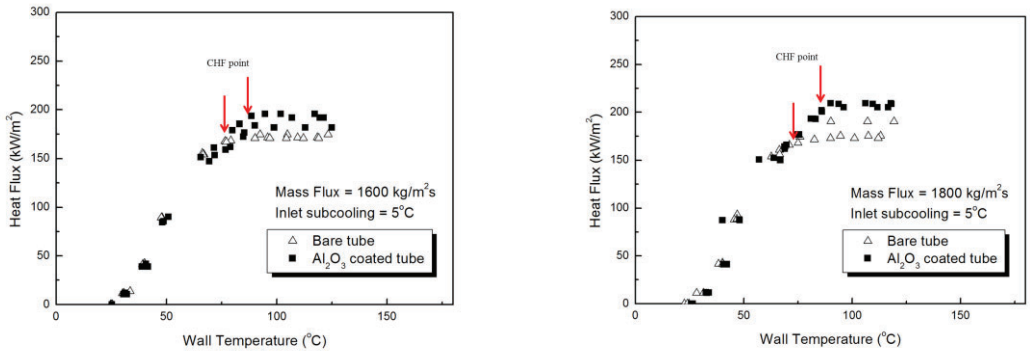

(a) **(b)**

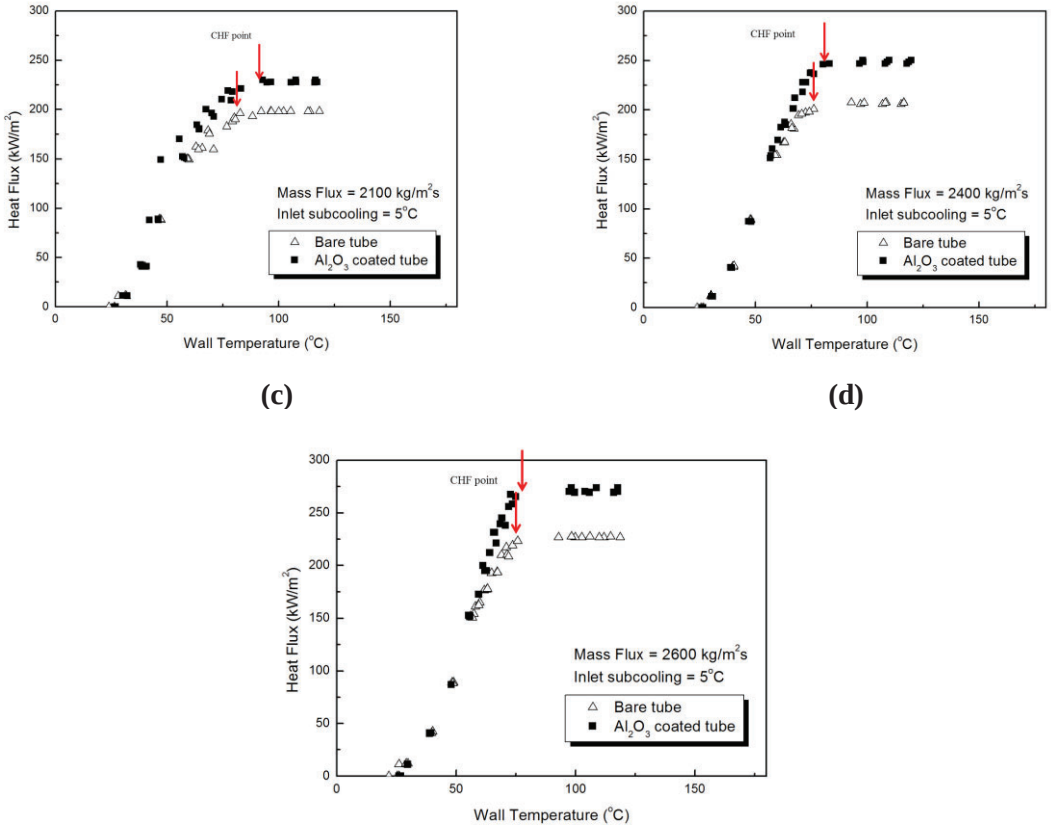

Figure 6. Boiling curves for bare tube and Al_2O_3 coated tube at different mass fluxes: (a) G=1600kg/m^{2}s (b) G=1800kg/m^{2}s (c) 2100kg/m^{2}s (d) 2400kg/m^{2}s (e) 2600kg/m^{2}s.

The CHF data obtained on bare and nanoparticles-coated surfaces according to mass fluxes are shown in Fig. 7. As the mass flux increases, CHF increases due to the larger heat capacity and better liquid supply of fluid. The parametric trend is also shown for the nanoparticle-coated surface. Interestingly, for all mass flux conditions, CHFs were enhanced on Al_2O_3 nanoparticle-coated surface compared to those of bare surface, even the coating layer thickness is in nano-scale. The nanoparticle-coated surface shows CHF enhancement up to 17% compared to bare surface for each corresponding mass flux condition. Considering the high wettability performance of R123, those CHF enhancements are attributed to structure changes, especially porous structures of heater surfaces by deposited nanoparticles. Fig. 8 shows the flow boiling CHF enhancement ratios which are defined as CHF on the Al_2O_3 nanoparticles-coated surface over CHF on the bare surface, with an increasing mass flux from 1600 to 2600 kg/m^{2}s.

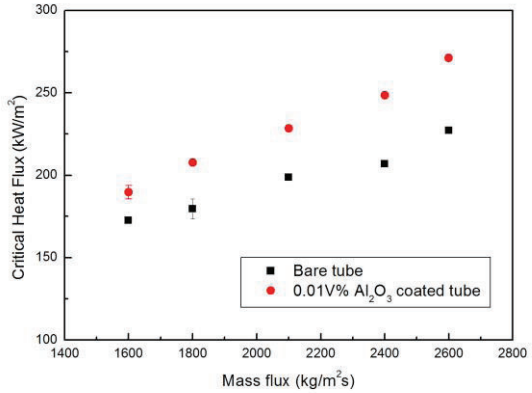

Figure 7. Critical heat flux of R123 on the bare and Al_2O_3 nanoparticle-coated test sections with mass flux.

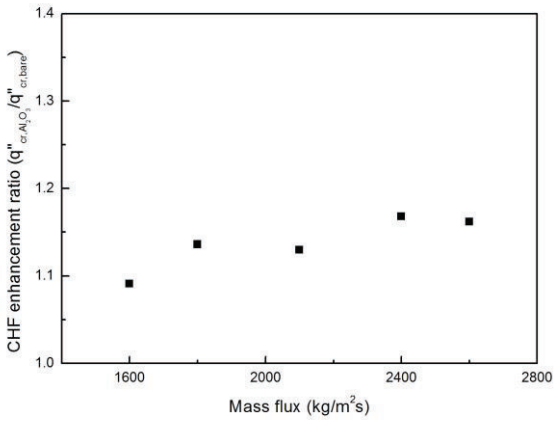

Figure 8. CHF enhancement ratio of R123 with mass flux.

Based on the sublayer dryout model [3], interruption of liquid supply to sublayer enlarges the dry patches leading to CHF. Then maintenance of liquid supply to sublayer after detaching of the vapor bubble, called rewetting process, can delay CHF. Assuming liquid supply is pumped by capillary force and gravitational force, the pressure drop by the liquid flow through the pores can be modeled using the Darcy-Ergun momentum relation [26, 27]

$$-\nabla p_l + \rho_l \hat{g} - \frac{\mu_l}{K}\langle \hat{u}_l \rangle - \frac{C_E}{K^{1/2}} \rho_l \left|\langle \hat{u}_l \rangle\right| \langle \hat{u}_l \rangle = 0 \tag{6}$$

where $<u_l>$ is the volume-averaged liquid velocity vector through liquid saturated region within the porous-layer coating, K is the media permeability, C_E is the Ergun coefficient. K and C_E are defined by Carmen-Kozeny model

$$K = \frac{\varepsilon^3 d^2}{180(1-\varepsilon)^2} \tag{7}$$

$$C_E = \left(\frac{0.018}{\varepsilon^3}\right)^{1/2} \tag{8}$$

To reduce the Darcy-Ergun momentum relation into the function of porous structure, Leverett J-function was introduced. The Leverett J-function expresses the capillary pressure through porous stack using the liquid saturation *(s)*, porosity, permeability, and wettability [26].

$$p_g - p_l = p_c = J(s)\frac{\sigma\cos\theta_c Z(\theta_c)}{\left(K/\varepsilon\right)^{1/2}} = C_J\frac{\sigma}{\left(K/\varepsilon\right)^{1/2}} \tag{9}$$

where θ_c is the contact angle, $Z(\theta_c)$ is the Melrose function assumed to 1, $J(s)$ is the Leverett function assumed to constant value of 0.53 [27].

Because capillary force becomes dominant in porous media, neglecting gravitational force produce the liquid velocity through the porous media

$$\left\langle \hat{u}_l \right\rangle = \frac{K^{1/2}}{2C_E\rho_l}\left[\left(\frac{\mu_l^{\,2}}{K^2} + \frac{2.12C_E\rho_l\sigma}{K^{1/2}\left(K/\varepsilon\right)^{1/2}l_m}\right)^{1/2} - \frac{\mu_l}{K}\right] \tag{10}$$

Finally, the local rate of liquid supply from the porous-layer to the heating surface is given by

$$\dot{m} = \rho_l A_{po}\left\langle u_l \right\rangle \tag{11}$$

Based on a local energy balance between liquid entering the micro-porous layer and sublayer, and the rate of the liquid depletion, local CHF occurrence is defined as [28]

$$\frac{q''_{CHF}A_w}{h_{fg}} = \rho_l\left\langle u_l\right\rangle\delta_m l + \rho_l\frac{K^{1/2}}{2C_E\rho_l}\left[\left(\frac{\mu_l^2}{K^2} + \frac{4C_E\rho_l C_J\sigma}{K^{1/2}(K/\varepsilon)^{1/2}l_m}\right)^{1/2} - \frac{\mu_l}{K}\right]\varepsilon\delta_p l \tag{12}$$

Using the assumption of porosity and diameter of porous particle as 0.6 and 1μm respectively, predicted CHF enhancement value by additional liquid supply of R123 through porous structure is 9 kW/m^2 from Eq. 1. The measured CHF enhancements are in the range of 17 - 44 kW/m^2 with increasing mass flow rate. The predicted CHF value by existing Yang's model shows difference with measured CHF value. Because the existing model was developed in pool boiling concept, modified model considering bulk liquid flow is needed to predict CHF enhancement by porous structure well. Because the bulk liquid velocity can determine the pressure difference through the porous media, it is suggested that capillary pressure function may contain bulk liquid velocity factor in itself like

$$p_c = 0.53\frac{\sigma}{\left(K/\varepsilon\right)^{1/2}}f(u_l) \tag{13}$$

where $f(u_l)$ is a multiplier factor function of bulk liquid velocity

Due to the insufficient experimental data and quantification of each parameter, a clearer explanation of enhanced rewetting process by nanoparticles deposited on the surface couldn't be achieved exactly despite almost same order of ~kW/m^2. With considering the bulk liquid velocity factor, further studies on CHF data for the various types of fluid and surface and clear quantification of surface parameter like porosity and diameter of porous particle will be desirable.

6. CONCLUSIONS

The CHF enhancement phenomena in R123 refrigerant on a bare and Al_2O_3 nanoparticles-coated heater were investigated according to mass flux. The nanoparticles-coated surface shows little difference in heat transfer coefficient, while CHF was enhanced up to 17% compared to bare surface. Due to the high wettability of R123 working fluid, the porosity and capillarity were assumed to be the key parameters for CHF enhancement. Porous structure by nanoparticles deposited on the surface provides the enhancement of rewetting process induced by increased capillary action. The predicted CHF value by existing theoretical model using capillary action through porous structure shows difference with measured CHF value. Because the existing model was developed in pool boiling concept, modified model considering bulk liquid flow is needed to predict CHF enhancement by porous structure well. Further studies on CHF data for the various types of fluid and surface and clear quantification of surface parameter like porosity and diameter of porous particle will be expected.

NOMENCLATURE (IF NEEDED)

A_s	total heated surface area [m^2]
A_w	wetted surface area [m^2]
A_{po}	area of porous media [m^2]
C_E	Ergun coefficient
$c_{p,f}$	heat capacity of liquid [kJ/kgK]
d	diameter of porous particle [m]
D_o	outer diameter of test section [m]
D_i	inner diameter of test section [m]
G	mass flux [kg/m^{2}s]
h_{fg}	latent heat of the liquid [kJ/kg]
I	current [A]
J	Leverett function
K	absolute permeability tensor [m^2]
k_c	thermal conductivity [W/mK]
$L_{eff,h}$	effective heated length of the test section [m]
l_m	length of media [m]
m_f	mass flow rate [kg/s]
P	input power [W]
p_c	capillary pressure [Pa]
p_g	vapor pressure [Pa]
p_l	liquid pressure [Pa]
Q_{net}	net input power [W]
q''_c	critical heat flux [kW/m^2]
q''_{eff}	effective heat flux [kW/m^2]
$\dot{q}$	linear heat rate [kW/m]
T_{sat}	saturation temperature of liquid [°C]
$T_{wall,out}$	outer wall temperature [°C]
T_{wall}	inner wall temperature [°C]

T_L local mean bulk temperature [°C]
T_{in} liquid inlet temperature [°C]
ΔT_{sub} inlet subcooling [°C]
u velocity [m/s]
$\langle u_l \rangle$ volume-averaged liquid velocity vector through liquid saturated region within the porous-layer coating [m/s]
V voltage [V]
X_e outlet quality
Z Melrose function
δ_b porous coating layer thickness [m]
ε porosity, or area fraction
θ_c static contact angle
μ_l dynamic viscosity of liquid [kg/m s]
ρ_l liquid density[kg/m^3]
σ surface tension of the liquid [N s/m^2]

ACKNOWLEDGMENTS

This work was supported by the Nuclear Energy Research Program through the National Research Foundation of Korea (NRF) funded by the Ministry of Science, ICT, and Future Planning (2013M2A8A1041442, 2013M2B2B1075734, 2013M2B2A4041473).

REFERENCES

1. J. Buongiorno, L. Hu, S. J. Kim, R. Hannink, B. Truong, E. Forrest, "Nanofluids for Enhanced Economics and Safety of Nuclear Reactors: An Evaluation of the Potential Features, Issues, and Research Gaps", *Nuclear Technology*, **162,** pp.80-91 (2008).
2. J. Weisman, B.S. Pei, "Prediction of critical heat flux in flow boiling at low quality". *Int. J. Heat Mass Transf.*, **26**, pp.1463–1477 (1983).
3. C. H. Lee, I. Mudawwar, "A Mechanistic Critical Heat Flux Model for Subcooled Flow Boiling based on Local Bulk Flow Conditions", *Int. J. Multiphase Flow*, **14**, pp.711-728 (1988).
4. S. M. You, J. H. Kim, K. H. Kim, "Effect of nanoparticles on critical heat flux of water in pool boiling heat transfer", *Appl. Phys, Lett.*, **83,** pp.3374–3376 (2003).
5. P. Vassallo, R. Kumar, S. D'Amico, "Pool boiling heat transfer experiments in silica-water nano-fluids", *Int. J. Heat mass Transfer*, **47,** pp.407-411 (2004).
6. I. C. Bang, S. H. Chang, "Boiling heat transfer performance and phenomena of Al_2O_3-water nano-fluids from a plain surface in a pool", *Int. J. Heat mass Transfer*, **48,** pp.2407-2419 (2005).
7. D. Wen, Y. Ding, "Experimental investigation into the pool boiling heat transfer of aqueous based γ-alumina nanofluids", *Journal of Nanoparticle Research*, **7,** pp.265-274 (2005).
8. H. Kim, J. Kim, M. Kim, "Experimental study on CHF characteristics of water-TiO_2 nanofluids", *Nuclear Engineering and Technology*, **38**, pp.61-68 (2006).
9. S. J. Kim, I. C. Bang, J. Buongiorno, L. W. Hu, "Surface wettability change during pool boiling of nanofluids and its effect on critical heat flux", *Int. J. of Heat and Mass Transfer*, **50,** pp.4105-4116 (2007).
10. S. J. Kim, T. McKrell, J. Buongiorno, L. W. Hu, "Alumina nanoparticles enhance the flow boiling critical heat flux of water at low pressure", *Journal of Heat Transfer*, **130,** pp.044501-1 – 044501-3 (2008).
11. S. J. Kim, T. McKrell, J. Buongiorno, L. W. Hu, "Experimental study of flow critical heat flux in alumina-water, zinc-oxide-water, and diamond-water nanofluids", *Journal of Heat Transfer*, **131**, pp.043204-1 – 043204-7 (2009).

12. T. I. Kim, Y. H. Jeong, S. H. Chang, "An experimental study on CHF enhancement in flow boiling using Al_2O_3 nano-fluid", *Int. J. Heat and Mass Transfer*, **53**, pp.1015-1022 (2010).
13. S. W. Lee, S. D. Park, S. Kang, S. M. Kim, H. Seo, D. W. Lee, I. C. Bang, "Critical heat flux enhancement in flow boiling of Al_2O_3 and SiC Nanofluids under low pressure and low flow conditions", *Nuclear Engineering and Technology*, **44**, pp.429-436 (2012).
14. J. Chen, *On the interaction between fuel crud and water chemistry in nuclear plants*, SKI report 00:5, Studsvik, Nykoping, Sweden (2000).
15. J. Buongiorno, "Can corrosion and CRUD actually improve safety margins in LWRs?", *Annals of Nuclear Energy*, 63, pp.9-21 (2014).
16. M. S. Sarwar, Y. H. Jeong, S. H. Chang, "Subcooled flow boiling CHF enhancement with porous surface coatings", *Int. J. Heat and Mass Transfer,* **50**, pp.3649-3657 (2007).
17. B. Truong, L. W. Hu, J. Buongiorno, T. McKrell, "Alumina nanoparticle pre-coated tubing enhancing subcooled flow boiling critical heat flux", *Proceedings of the ASME 2009 2nd Micro/Nanoscale Heat & Mass Transfer International Conference*, China, Shanghai, December 18-21 (2009).
18. T. I. Kim, W. J. Chang, S H. Chang, "Flow boiling CHF enhancement using Al2O3 nanofluid and an Al_2O_3 nanoparticle deposited tube", *Int. J. Heat and Mass Transfer*, **54**, pp.2021-2025 (2011).
19. A. Kosar, Y. Peles, "Critical heat flux of R-123 in silicon-based microchannels", *Journal of Heat Transfer*, **129**, pp.844-851 (2007).
20. A. P. Roday, M. K. Jensen, "Study of the critical heat flux condition with water and R-123 during flow boiling in microtubes. Part I: Experimental results and discussion of parametric effects", *Int. J. Heat and Mass Transfer*, **52**, pp.3235-3249 (2009).
21. A. P. Roday, M. K. Jensen, "Study of the critical heat flux condition with water and R-123 during flow boiling in microtubes. Part II: Comparison of data with correlations and establishment of a new subcooled CHF correlation", *Int. J. Heat and Mass Transfer*, **52**, pp.3250-3256 (2009).
22. H. Seo, J. H. Chu, S. Y. Kwon, I. C. Bang, "Pool boiling CHF of reduced graphene oxide, graphene, and SiC-coated surfaces under highly wettable FC-72", *Int. J. Heat and Mass Transfer*, **82**, pp.490-502 (2015).
23. M. T. Al-Garni, B. D. Al-Anazi, "Investigation of wettability effects on capillary pressure, and irreducible saturation for Saudi crude oils, using rock centrifuge", *Oil and Gas Business* (2008).
24. K. M. Kim, S. W. Lee, I. C. Bang, "Effects of SiC and Graphene-Oxide Nanoparticles-Coated Surfaces on Quenching Performance", *ATH2014*, USA, Nevada, Reno, June 15-19 (2014).
25. S. Fischer, E. M. Slomski, P. Stephan, M. Oechsner, "Enhancement of nucleate boiling heat transfer by micro-structured chromium nitride surfaces", *Journal of Physics: Conference Series*, **395**, pp.012128 (2012).
26. M. Kaviany, *Principles of Heat Transfer in Porous Media*, Springer, New York (1999).
27. S. G. Liter, M. Kaviany, "Pool-boiling CHF enhancement by modulated porous-layer coating: theory and experiment", *Int. J. Heat and Mass Transfer*, **44**, pp.4287-4311 (2001).
28. J. Yang, F. B. Cheung, "A hydrodynamic CHF model for downward facing boiling on a coated vessel", *Int. J. Heat and Fluid Flow*, **26**, pp.474-484l (2005).